Nonlinear variational method for predicting fast collisionless magnetic reconnection

M. Hirota[1], P. J. Morrison[2], Y. Ishii[1], M. Yagi[1] and N. Aiba[1]

[1] Japan Atomic Energy Agency, Rokkasho, Aomori 039-3212, Japan
[2] University of Texas at Austin, Austin, Texas 78712 USA

E-mail: `hirota.makoto@jaea.go.jp`

Abstract. A mechanism for fast magnetic reconnection in collisionless plasma is studied for understanding sawtooth collapse in tokamak discharges. Explosive growth of the tearing mode driven by electron inertia is analytically estimated by using an energy principle with a nonlinear displacement map. Decrease of the potential energy in the nonlinear regime (where the island width exceeds the electron skin depth) is found to be steeper than in the linear regime, resulting in accelerated reconnection. Release of free energy by such ideal fluid motion leads to unsteady and strong convective flow, which is not deterred by the small dissipation effects in high-temperature tokamak plasmas. Direct numerical simulation in slab geometry substantiates the theoretical prediction of the nonlinear growth.

1. Introduction

Sawtooth collapse in tokamak plasmas has been a puzzling phenomenon for decades. Although the $m = 1$ kink-tearing mode is essential for the onset of this dynamics, Kadomtsev's full reconnection model [1] and the nonlinear growth of the resistive $m = 1$ mode [2] (both based on resistive magnetohydrodynamic (MHD) theory) fail to explain the short collapse times ($\sim 100\mu s$) as well as the partial reconnections observed in experiments [3, 4, 5]. Since resistivity is small in high-temperature tokamaks, two-fluid effects are expected to play an important role for triggering *fast* (or *explosive*) magnetic reconnection as in solar flares and magnetospheric substorms.

In earlier works [6, 7], the linear growth rate of the kink-tearing mode in the collisionless regime has been analyzed extensively by using asymptotic matching, which shows an enhancement of the growth rate due to two-fluid effects, even in the absence of resistivity. Furthermore, direct numerical simulations [8, 9, 10] of two-fluid models show acceleration of reconnection in the nonlinear phase, even though realistic two-fluid simulation of high-temperature tokamaks is still a computationally demanding task (especially when the resistive layer width is smaller than the electron skin depth $d_e \sim$ 1mm). These simulation studies, as a rule, indicate explosive tendencies of collisionless reconnection.

However, theoretical understanding of such explosive phenomena is not yet established due to the lack of analytical development. In the neighborhood of the boundary (or reconnecting) layer, a perturbative approach breaks down at an early nonlinear phase and, consequently, asymptotic matching requires a fully nonlinear inner solution [11]. Moreover, in contrast to the quasi-equilibrium analysis developed for resistive reconnection [2, 12], the explosive process of collisionless reconnection should be a nonequilibrium problem, in which inertia is not negligible in the force balance and hence leads to acceleration of flow. Thus, the convenient assumption of *steady* reconnection is no longer appropriate. Recent theories [13, 14, 15] emphasize the Hamiltonian nature of two-fluid models and try to gain deeper understanding of collisionless reconnection in the ideal limit.

The purpose of the present work is to predict the explosive growth of the kink-tearing mode analytically by developing a new nonlinear variational technique that is based on a generalization of the MHD energy principle [16, 17] (for generalization see [18]). For simplicity, we concentrate on the effect of electron inertia, which is an attractive mechanism for triggering fast reconnection in tokamaks; estimates of the reconnection rate are favorable [19], nonlinear acceleration is possible [9], and even the more mysterious partial reconnection may be explained by an inertia-driven collapse model [20, 21]. While we address the same problem as that of Ref. [9], our estimated nonlinear growth is quantitatively different from that of this reference, and our result is confirmed by direct numerical simulation. This advance in nonlinear theory is indispensable for clarifying the acceleration mechanism of collisionless reconnection.

The present paper is organized as follows. In Sec. 2, we invoke a conventional 2D

slab model for electron inertia-driven reconnection and then construct its Lagrangian in terms of the fluid flow map (as in the ideal MHD theory [22, 23, 24]). In Sec. 3, we obtain the linear growth rate of the inertial tearing mode in the large-Δ' regime (corresponding to the $m = 1$ kink-tearing mode in tokamaks) by applying our energy principle to this two-fluid model. We show that a rather simple displacement field is enough to make the potential energy decrease ($\delta W < 0$) and to obtain a tearing instability whose growth rate agrees with the asymptotic matching result [6, 7]. Given these observations, we extend the energy principle to a nonlinear regime in Sec. 4, where the displacement (or the magnetic island width) is larger than d_e. Without relying on perturbation expansion, we directly substitute a form of the displacement map into the Lagrangian and attempt to minimize the potential energy W. We show that a continuous deformation of magnetic field-lines into a Y-shape [25] asymptotically leads to a steeper decrease of W than that of the linear regime, which is indeed found to be responsible for the acceleration phase. In Sec. 5, the effect of small dissipation on this fast reconnection are considered and implications of our results for sawtooth collapse are finally discussed.

2. Model equations and their Lagrangian description

We analyze the following vorticity equation and (collisionless) Ohm's law for the velocity field $\boldsymbol{v} = \boldsymbol{e}_z \times \nabla\phi(x, y, t)$ and magnetic field $\boldsymbol{B} = \nabla\psi(x, y, t) \times \boldsymbol{e}_z + B_0\boldsymbol{e}_z$:

$$\frac{\partial \nabla^2 \phi}{\partial t} + [\phi, \nabla^2 \phi] + [\nabla^2 \psi, \psi] = 0, \tag{1}$$

$$\frac{\partial(\psi - d_e^2 \nabla^2 \psi)}{\partial t} + [\phi, \psi - d_e^2 \nabla^2 \psi] = 0, \tag{2}$$

where $[f, g] = (\nabla f \times \nabla g) \cdot \boldsymbol{e}_z$. As noted in Sec. 1, the parameter d_e denotes the electron skin depth, which is much smaller than the system size ($d_e \ll L$). Since the frozen-in flux for Eq. (2) is not the magnetic flux ψ, but the electron canonical momentum defined by $\psi_e = \psi - d_e^2 \nabla^2 \psi$, the effect of electron inertia permits magnetic reconnection within a thin layer ($\sim d_e$) despite a lack of resistivity in this model.

    In the same manner as in Ref. [9], we consider a static equilibrium state,

$$\phi^{(0)} = 0 \quad \text{and} \quad \psi^{(0)}(x) = \psi_0 \cos \alpha x, \tag{3}$$

on a doubly-periodic domain $D = [-L_x/2, L_x/2] \times [-L_y/2, L_y/2]$ (where $\alpha = 2\pi/L_x$), and analyze the nonlinear evolution of the tearing mode with wavenumber in the y-direction $k = 2\pi/L_y$ at its early linear stage. For sufficiently small k such that

$$\pi k^2/4\alpha^3 = L_x^3/8L_y^2 \ll d_e \ll L_x, \tag{4}$$

this instability is similar to the $m = 1$ kink-tearing mode in tokamaks (which belongs to the large-Δ' regime; see Appendix A). Figure 1 shows contours of ψ calculated by direct numerical simulation, where ϵ denotes the maximum displacement in the x-direction. Our numerical code employs a spectral method in the y-direction with up to 200 modes and a finite difference scheme in the x-direction with uniform grid points $\sim 10,000$. The
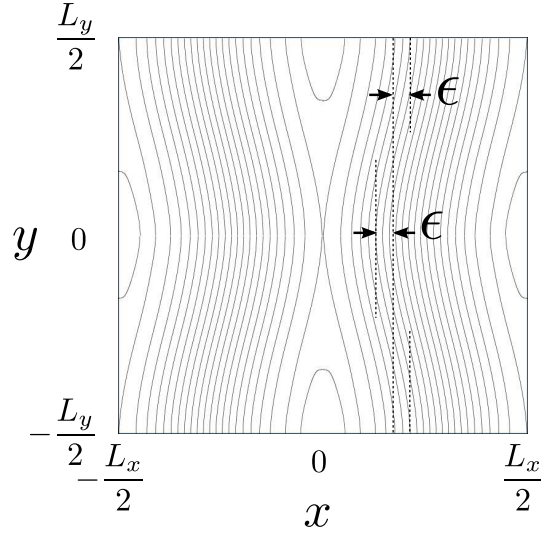
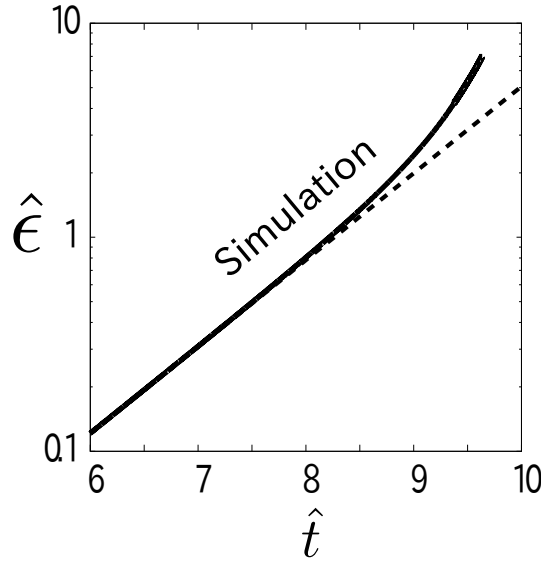**Figure 1.** Contours of ψ when $\epsilon = 4.2d_e$ ($d_e/L_x = 0.01$ and $L_y/L_x = 4\pi$)

Figure 2. Growth of $\hat{\epsilon} = \epsilon/d_e$ with respect to time $\hat{t} = t/\tau_0$ ($d_e/L_x = 0.01$ and $L_y/L_x = 4\pi$)

growth of ϵ accelerates when $\hat{\epsilon} = \epsilon/d_e > 1$, as shown in figure 2 (which is faster than exponential). In accordance with Ref. [9], a strong spike of electric current $J = -\nabla^2\psi$ develops inside the reconnecting layer and the width of this current spike continues to shrink as time progresses, unless a dissipative term is added to (2). Therefore, direct numerical simulation of (1) and (2) inevitably terminates when this coherent energy cascade reaches the limit of resolution.

In order to clarify the free energy source of this explosive instability, we solve the conservation law (2) for $\psi_e = \psi - d_e^2\nabla^2\psi$ by introducing an incompressible flow map $\boldsymbol{G}_t : D \to D$, which depends on time and corresponds to the identity map when

$t = -\infty$ ($\boldsymbol{G}_{-\infty} = \mathrm{Id}$). Let $(x, y)(t) = \boldsymbol{G}_t(x_0, y_0)$ be orbits of fluid elements labeled by their position (x_0, y_0) at $t = -\infty$. Then, the velocity field (or ϕ) is related to $\boldsymbol{G}_t$ as

$$\frac{\partial \boldsymbol{G}_t}{\partial t}(x_0, y_0) = \boldsymbol{e}_z \times \nabla\phi(x, y, t). \tag{5}$$

Regarding $\boldsymbol{G}_t$ as an unstable fluid motion emanating from the equilibrium state (3), we can solve Ohm's law (2) by

$$\psi_e(x, y, t) = \psi_e(\boldsymbol{G}_t(x_0, y_0), t) = \psi_e^{(0)}(x_0), \tag{6}$$

where $\psi_e^{(0)}(x) = (1 + d_e^2\alpha^2)\psi_0 \cos(\alpha x)$. Both ϕ and ψ_e (or ψ) are thus expressed in terms of $\boldsymbol{G}_t$. By adapting Newcomb's Lagrangian theory [22], we define the Lagrangian for the fluid motion $\boldsymbol{G}_t$ as

$$L[\boldsymbol{G}_t] = K[\boldsymbol{G}_t] - W[\boldsymbol{G}_t], \tag{7}$$

where

$$K[\boldsymbol{G}_t] = \frac{1}{2} \int_D |\nabla\phi|^2 d^2x, \tag{8}$$

$$W[\boldsymbol{G}_t] = \frac{1}{2} \int_D \left(|\nabla\psi|^2 + d_e^2|\nabla^2\psi|^2 \right) d^2x. \tag{9}$$

Then, the variational principle $\delta \int L[\boldsymbol{G}_t]dt = 0$ with respect to $\delta\boldsymbol{G}_t$ yields the vorticity equation (1).

Since the Hamiltonian corresponds to $H = K + W$ (= const.), we note that W plays the role of potential energy and the equilibrium state (3) initially stores it as free energy. In the same spirit as the energy principle [16, 17], if the potential energy decreases ($\delta W < 0$) for some displacement map $\boldsymbol{G}_t$, then such a perturbation will grow with the release of free energy. In comparison to the ideal MHD case [22], the electron's *kinetic* energy $(1/2) \int_D d_e^2 J^2 d^2x$ appears as a part of the potential energy, because we have treated the conservation law of electron's momentum ψ_e as a kinematic constraint. To avoid confusion, we will refer to this $(1/2) \int_D d_e^2 J^2 d^2x$ as current energy in this work.

3. Energy principle for linear stability analysis

In our linear stability analysis, the equilibrium state is perturbed by an *infinitesimal* displacement, $\boldsymbol{G}_t(x_0, y_0) = (x_0, y_0) + \boldsymbol{\xi}(x_0, y_0, t)$, where $\boldsymbol{\xi}$ is a divergence-free vector field on D. For a given wavenumber $k = 2\pi/L_y$, we seek a linearly unstable tearing mode in the form

$$\boldsymbol{\xi}(x, y, t) = \nabla\left[\epsilon(t)\hat{\xi}(x)\frac{\sin ky}{k}\right] \times \boldsymbol{e}_z, \tag{10}$$

with a growth rate $\epsilon(t) \propto e^{\gamma t}$. We normalize the eigenfunction $\hat{\xi}(x)$ by $\max|\hat{\xi}(x)| = 1$ so that $\epsilon(t)$ is equal to the maximum displacement in the x-direction and, hence, measures the half width of the magnetic island.

Upon omitting "(0)" from equilibrium quantities, $\psi^{(0)}$, $\psi_e^{(0)}$, $J^{(0)}$, etc., to simplify the notation, the eigenvalue problem can be written in the form

$$-\left[\left(\gamma^2/k^2 + \psi_e'^2\right)\hat{\xi}'\right]' + k^2\left(\gamma^2/k^2 + \psi_e'^2\right)\hat{\xi} = d_e^2\psi_e'J'''\hat{\xi} + d_e^2\psi_e'\nabla^2\frac{1}{1 - d_e^2\nabla^2}\nabla^2(\psi_e'\hat{\xi}), \tag{11}$$
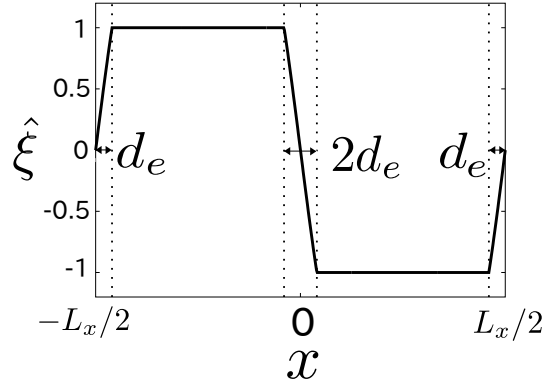
Figure 3. Test function that mimics the unstable tearing mode

where ∇^2 should be interpreted as $\nabla^2 = \partial_x^2 - k^2$ and the prime $(')$ denotes the x derivative. Note, (11) ranks as a fourth order ordinary differential equation (unless $d_e = 0$) because of the integral operator $(1 - d_e^2\nabla^2)^{-1}$ on the right hand side. By multiplying the both sides of (11) by $\hat{\xi}$ and integrating over the domain, we get $-\gamma^2 I^{(2)} = W^{(2)}$, where

$$I^{(2)} = \int_{-L_x/2}^{L_x/2} dx \frac{1}{k^2} \left(|\hat{\xi}'|^2 + k^2|\hat{\xi}|^2 \right), \tag{12}$$

$$W^{(2)} = \int_{-L_x/2}^{L_x/2} dx \left[-(\psi_e'\hat{\xi}) \frac{\nabla^2}{1 - d_e^2\nabla^2} (\psi_e'\hat{\xi}) + \psi_e'\psi_e'''|\hat{\xi}|^2 \right]. \tag{13}$$

The functionals $\gamma^2 I^{(2)}$ and $W^{(2)}$ are, respectively, related to the kinetic and potential energies for the linear perturbation. Hence, by invoking the energy principle [16] (or the Rayleigh-Ritz method), we can search for the most unstable eigenvalue ($\gamma > 0$) by minimizing $W^{(2)}/I^{(2)}$ with respect to $\hat{\xi}$.

Because we assume the ordering (4) that corresponds to the kink-tearing mode, the eigenfunction $\hat{\xi}$ is approximately constant except for thin boundary layers at $x = 0, \pm L_x/2$ and has discontinuities around them because of the singular property of (11) in the limit of $(\gamma/k), k, d_e \to 0$. The electron inertia effect would *smooth out* these discontinuities. For this reason, we choose a piecewise-linear test function shown in figure 3. In a region containing the boundary layer at $x = 0$, it is given explicitly by

$$\hat{\xi}(x) = \begin{cases} 1 & \text{for } x < -d_e \\ -x/d_e & \text{for } -d_e < x < d_e \\ -1 & \text{for } d_e < x. \end{cases} \tag{14}$$

The outer layers at $x = \pm L_x/2$ are equivalent owing to the periodicity and symmetry of the problem. By substituting this function into (12) and (13), we can make $W^{(2)}$ negative and keep $I^{(2)}$ finite; i.e., we obtain

$$I^{(2)} \simeq \frac{4}{d_e k^2} \quad \text{and} \quad W^{(2)} \simeq -2\left(\frac{1}{3} + 9e^{-2}\right) d_e \tau_H^{-2}, \tag{15}$$
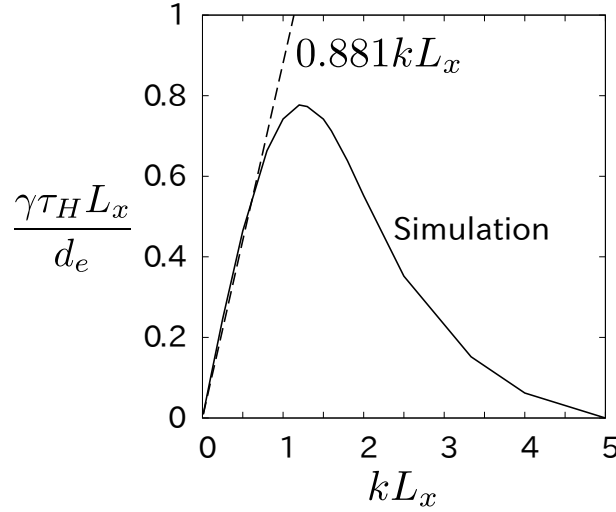
Figure 4. Dependence of linear growth rate γ on k (for $d_e/L_x = 0.01$)

where $\tau_H^{-1} = \alpha^2 \psi_0 = B_y'|_{x=0}$ and we have extracted only the leading-order term (see Appendix A for detail). The linear growth rate is therefore estimated as follows:

$$\gamma = \sqrt{-W^{(2)}/I^{(2)}} = \sqrt{0.776\tau_0^{-2}} = 0.881\tau_0^{-1}, \tag{16}$$

where $\tau_0^{-1} = d_e k \tau_H^{-1}$. This result agrees with the general dispersion relation derived by asymptotic matching [6, 7]. Of course, our analytical estimate of the growth rate depends on how good the chosen test function mimics the genuine eigenfunction. Nevertheless, the result predicted by the simple function (14) shows satisfactory agreement with the numerically calculated growth rate (see figure 4) in the small k region corresponding to the ordering (4). In the following simulations, we always put $kL_x = 0.5$.

4. Variational estimate of explosive nonlinear growth

Next, we consider the nonlinear phase of the linear instability discussed above. We remark in advance that a higher-order perturbation analysis of the Lagrangian (i.e., weakly nonlinear analysis) will not be successful, as was already pointed out by Rosenbluth et al. for the case of the ideal internal kink mode [11]. For example, the Lie-series expansion [26] of (6) leads to

$$\psi_e = \psi_e^{(0)} + \boldsymbol{\xi} \cdot \nabla \psi_e^{(0)} + \frac{1}{2}\boldsymbol{\xi} \cdot \nabla(\boldsymbol{\xi} \cdot \nabla \psi_e^{(0)}) + O(\epsilon^3/d_e^3). \tag{17}$$

Thus, such a perturbation expansion easily fails to converge when the displacement ϵ (or the island width) reaches the boundary layer width $\sim d_e$, due to a steep gradient $\partial_x \hat{\xi} \sim \hat{\xi}/d_e$ of the eigenfunction inside the layers (see figure 3). Naive perturbation analysis is, therefore, only valid for $0 \leq \epsilon \ll d_e$, while ϵ actually exceeds d_e without saturation as in figure 2.

To avoid difficulties of a rigorous fully-nonlinear analysis, we again take advantage of a variational approach. Namely, we devise a trial fluid motion (parameterized by the
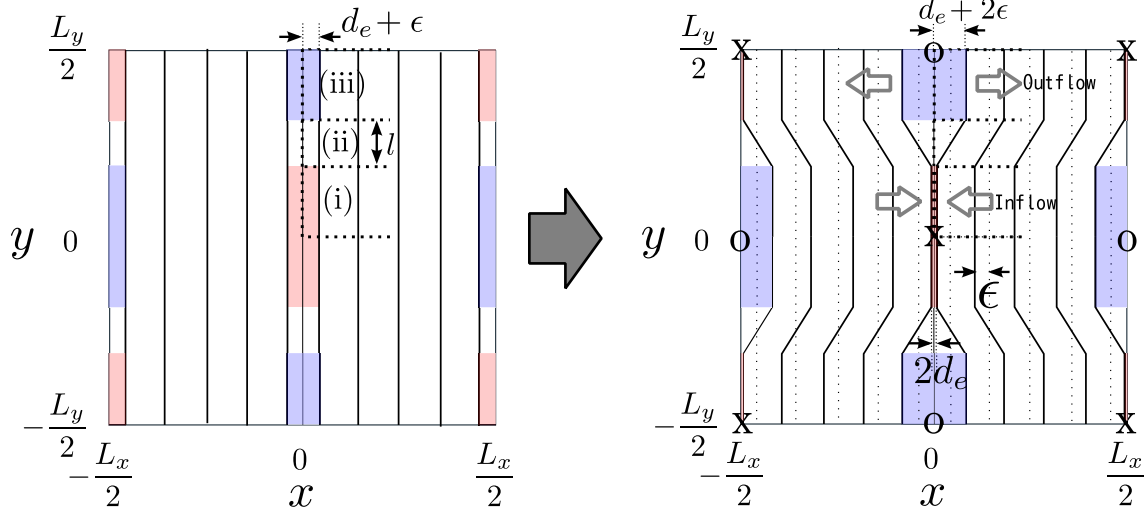
Figure 5. Deformation of contours of ψ_e by the displacement map (18)

amplitude ϵ) that tends to decrease the potential energy W as much as possible. When such a motion is substituted into the Lagrangian (7), it is expected to be nonlinearly unstable.

Owing to the symmetry of the mode pattern, it is enough to discuss the boundary layer at $x = 0$ and, moreover, focus on only the 1st quadrant, $0 < x$ and $0 < y < L_y/2$. In a heuristic manner, based on the above linear analysis and simulation results, we consider a displacement map $\boldsymbol{G}_\epsilon : (x_0, y_0) \mapsto (x, y)$, where the displacement in the x direction is prescribed by

$$x = \begin{cases} g_\epsilon(x_0) & \text{for (i) } 0 < y_0 < \frac{L_y}{4} - \frac{l}{2} \\ x_0 + \dfrac{2}{l}\left(y_0 - \dfrac{L_y}{4}\right)\left(x_0 - g_\epsilon(x_0)\right) & \text{for (ii) } \frac{L_y}{4} - \frac{l}{2} < y_0 < \frac{L_y}{4} + \frac{l}{2} \\ 2x_0 - g_\epsilon(x_0) & \text{for (iii) } \frac{L_y}{4} + \frac{l}{2} < y_0 < \frac{L_y}{2}. \end{cases} \tag{18}$$

The regions (i)-(iii) are indicated in figure 5(left) and we furthermore define g_ϵ as

$$g_\epsilon(x_0) = \begin{cases} e^{-\hat{\epsilon}}x_0 & \text{for } 0 < x_0 < d_e \\ d_e e^{\frac{x_0 - \epsilon}{d_e} - 1} & \text{for } d_e < x_0 < d_e + \epsilon \\ x_0 - \epsilon & \text{for } d_e + \epsilon < x_0. \end{cases} \tag{19}$$

As illustrated in figure 5, this displacement map deforms the contours of ψ_e into a pattern with Y-shaped ends [25]. In a nonlinear regime with $d_e \ll \epsilon \ll L_x$, we find that such a deformation decreases the potential energy (9) in a manner that is close to the steepest descent. Leaving the detailed estimate of δW to Appendix B, our reasoning process can be detailed as follows.

First, in the region (i), the flux ψ_e of the red area of figure 5(left) is squeezed into a thin boundary layer whose width is $2d_e$ in figure 5(right). On the other hand, the flux is expanded in the region (iii) and the blue area of figure 5(left) is almost doubled in
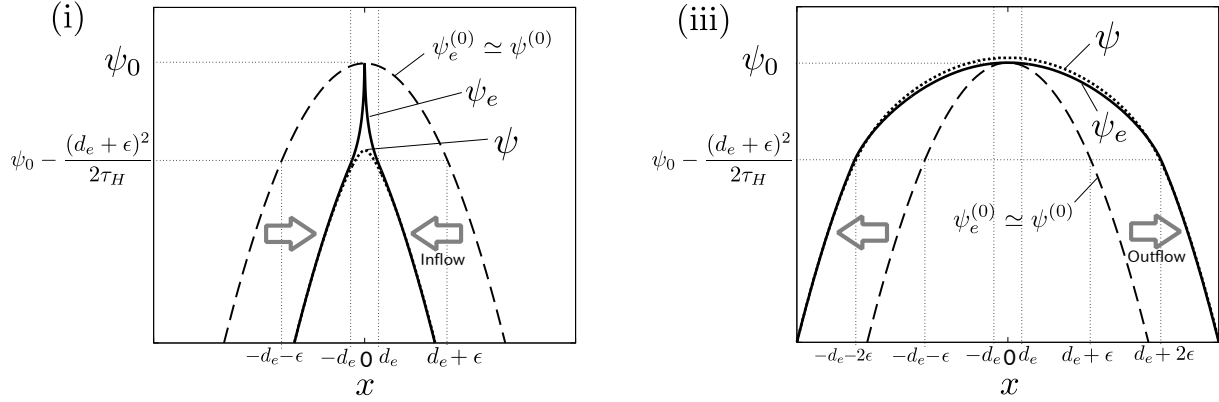
Figure 6. Changes of ψ_e and ψ from the equilibrium state $\psi_e^{(0)} \simeq \psi^{(0)}$ around the domains (i) and (iii), due to the displacement map (18) with $\epsilon = 5d_e$.

figure 5(right). The resultant forms of ψ_e and ψ are shown in figure 6. Since the magnetic flux ψ approximately conforms to ψ_e except in the neighborhood of the boundary layers, both deformations tend to decrease the magnetic energy $(1/2) \int |\nabla \psi|^2 d^2 x$ as ϵ^3 when $d_e \ll \epsilon \ll L_x$. This overall loss of magnetic energy is the earmark of collisionless magnetic reconnection.

Inside the boundary layers [i.e., the red regions in figure 5(right)], care must be taken in representing the formation of the strong current spikes [9], which are observed as $J = (\psi_e - \psi)/d_e^2$ in figure 6(i). These spikes tend to increase the current energy $(1/2) \int d_e^2 J^2 d^2 x$ in (9). However, the asymptotic form of the current is approximated by a logarithmic function, $J \simeq \tau_H^{-1} \hat{\epsilon} \log |x/d_e|$ for $\hat{\epsilon} = \epsilon/d_e \gg 1$, and the current energy change is, at most, of the second order $O(\hat{\epsilon}^2)$. Therefore, in the regions (i) and (iii), the dominant contribution of the potential energy decreases at the rate of order $O(\hat{\epsilon}^3)$ despite the minor increase of the current energy.

Only in the intermediate region (ii) located between (i) and (iii), does the potential energy tend to increase due to the bending of magnetic field-lines over the distance l. But, we can minimize this contribution from the region (ii) by taking its width l to be sufficiently small: $l \ll L_y$. We are allowed to use this approximation as far as the ordering (4) is concerned; L_y is the longest scale length in this ordering and, in fact, $L_y \to \infty$ is similar to the behavior of the $m = 1$ kink-tearing mode.

By noting that there are, respectively, eight regions that are equivalent to (i) and (iii) in the whole domain D, analytical estimates given in Appendix B can be gathered into the following:

$$\delta W[\boldsymbol{G}_\epsilon] \simeq 8\delta W_{(\mathrm{i})} + 8\delta W_{(\mathrm{iii})} = -L_y \tau_H^{-2} d_e^3 \left[\frac{\hat{\epsilon}^3}{2} + O(\hat{\epsilon}^2) \right], \tag{20}$$

for $d_e \ll \epsilon \ll L_x$.

To evaluate the nonlinear growth rate of ϵ, it is necessary to estimate the kinetic energy. By introducing time-dependence in $\epsilon(t)$ via the displacement map (18), a

straightforward analysis (given in Appendix C) eventually results in

$$K[\boldsymbol{G}_{\epsilon(t)}] \simeq 8K_{(\mathrm{i})} + 8K_{(\mathrm{iii})} = \frac{\pi^2 \log 2}{6} L_y \tau_H^{-2} d_e^3 \left(\frac{d\hat{\epsilon}}{d\hat{t}}\right)^2, \tag{21}$$

where $\hat{t} = t/\tau_0$. This estimate is not remarkably different from that of the linear regime.

With these estimates, the Lagrangian (7) reduces to

$$L[\boldsymbol{G}_{\epsilon(t)}] \simeq \frac{\pi^2 \log 2}{6} L_y \tau_H^{-2} d_e^3 \left[\left(\frac{d\hat{\epsilon}}{d\hat{t}}\right)^2 - U(\hat{\epsilon})\right], \tag{22}$$

where the normalized potential energy is given by

$$U(\hat{\epsilon}) = -(3/\pi^2 \log 2)\hat{\epsilon}^3 + O(\hat{\epsilon}^2) = -0.439\hat{\epsilon}^3 + O(\hat{\epsilon}^2). \tag{23}$$

The equation of motion is, of course, $d^2\hat{\epsilon}/d\hat{t}^2 = F(\hat{\epsilon})$ with $F(\hat{\epsilon}) = -(1/2)dU/d\hat{\epsilon}$.

In the linear regime ($\epsilon \ll d_e$), we have already shown that the potential energy decreases as $U(\hat{\epsilon}) = -0.776\hat{\epsilon}^2$ and $\epsilon(t)$ grows exponentially. The steeper descent where $U(\hat{\epsilon}) = -0.439\hat{\epsilon}^3$ in the nonlinear regime ($d_e \ll \epsilon \ll L_x$) indicates an explosive growth of ϵ, namely, it reaches the order of the system size L_x during a finite time $\sim \tau_0$.

We remark that the nonlinear force $F(\hat{\epsilon}) \sim O(\hat{\epsilon}^2)$ obtained here is different from $F(\hat{\epsilon}) \sim O(\hat{\epsilon}^4)$ in the earlier theory by Ottaviani and Porcelli [9]. While similar fluid motion around the X and O points is considered in Ref. [9], they directly integrate the vorticity equation (1) over the quadrant $[0, L_x/2] \times [0, L_y/2]$ and arrive at an equation of motion $d^2\hat{\epsilon}/d\hat{t}^2 = F(\hat{\epsilon}) \sim O(\hat{\epsilon}^4)$. However, unless the assumed trial motion happens to be an exact solution, their treatment may lead to a wrong equation of motion that does not satisfy energy conservation. Moreover, their ansatz of the "fixed flow-pattern" is also found to be inappropriate in our trial-and-error process. If we try fixing the stream function ϕ throughout the linear and nonlinear regimes as

$$\phi(x, y, t) = \frac{d\epsilon}{dt}(t)\hat{\xi}(x)\frac{\sin ky}{k}, \tag{24}$$

with the same $\hat{\xi}(x)$ as (14), the contours of ψ_e are deformed into a mushroom-like shape as shown in figure 7. With this choice, the potential W does not continue to decrease – such a fixed flow-pattern merely circulates the flux ψ_e from the X point side to the O point side via the boundary layer.

In direct numerical simulation, we have calculated the potential energy $U(\hat{\epsilon})$ [or, equivalently, the kinetic energy $(d\hat{\epsilon}/d\hat{t})^2$] as a function of $\hat{\epsilon}$. As shown in figure 8, the decrease of $U(\hat{\epsilon})$ agrees with our scaling and does not support the scaling $U \sim -\hat{\epsilon}^5$ of Ref. [9].

5. Small dissipation

In this section, we consider the effect of small dissipation by introducing resistivity (η) and electron perpendicular viscosity (μ_e) into Ohm's law (2); i.e.,

$$\frac{\partial \psi_e}{\partial t} + \boldsymbol{v} \cdot \nabla \psi_e = -\eta J + \mu_e d_e^2 \nabla^2 J. \tag{25}$$
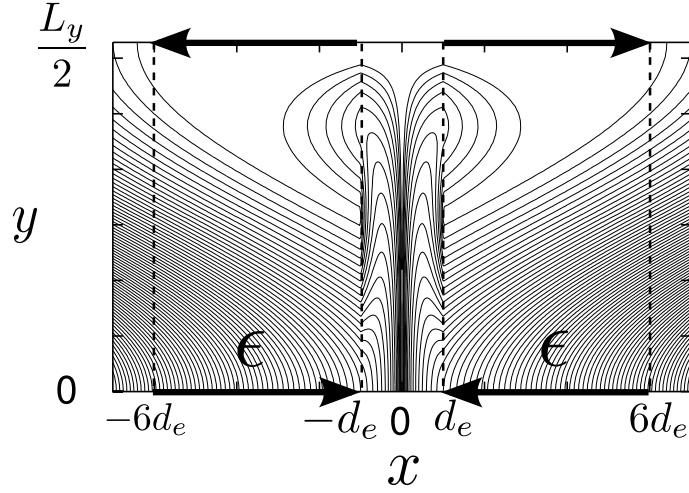
Figure 7. Contours of ψ_e convected by the fixed flow (24) (when $\epsilon = 5d_e$).
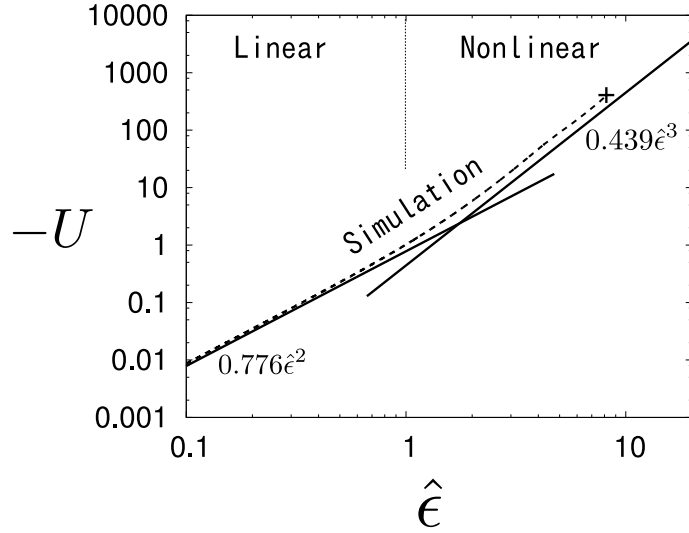

Figure 8. Potential energy $U(\hat{\epsilon})$ (where $d_e/L_x = 0.01$ and $L_y/L_x = 4\pi$ in simulation)

Both terms on the right hand side only dissipate the potential energy W. For sufficiently small η and μ_e, we can still employ the energy principle in the manner used to describe the resistive wall mode in Ref. [27]. Thus, the energy principle is extended as

$$-\gamma^2 I^{(2)} = W^{(2)} + W^{(2)}_{\text{dis}} + O(\eta^2, \mu_e^2), \tag{26}$$

where

$$W^{(2)}_{\text{dis}} = -\frac{1}{\gamma} \int_{-L_x/2}^{L_x/2} \left(\eta|\hat{J}|^2 + \mu_e d_e^2 |\nabla \hat{J}|^2 \right) dx < 0, \tag{27}$$

and

$$\hat{J} = \frac{\nabla^2}{1 - d_e^2 \nabla^2}(\psi'_e \hat{\xi}). \tag{28}$$

By substituting the same test function $\hat{\xi}$ of (14) into $W_{\text{dis}}^{(2)}$, the linear growth rate (16) is modified to

$$\gamma = 0.881\tau_0^{-1} + 0.367\tau_e^{-1} + 0.347\tau_d^{-1} + \tau_0^{-1}O\left(\frac{\tau_0^2}{\tau_e^2}, \frac{\tau_0^2}{\tau_d^2}\right), \tag{29}$$

where $\tau_e = d_e^2/\eta$ is the electron collision time and $\tau_d = d_e^2/\mu_e$ is the electron diffusion time over a distance d_e. Small η and μ_e, therefore, enhance the linear growth rate.

Now, let us interpret our result for tokamak parameters. Since $\tau_e/\tau_d \sim (\rho_e/d_e)^2$, where ρ_e is the electron gyroradius, the effect of electron viscosity is typically much smaller than that of resistivity, $\tau_e/\tau_d \ll 1$, in strongly magnetized plasmas in tokamaks.

However, the time scales τ_0 and τ_e can sometimes be similar in tokamak plasmas. For the $m = 1$ kink-tearing mode in tokamaks, $\tau_0^{-1} = d_e k \tau_H^{-1}$ corresponds to $\tau_0^{-1} = d_e q_1' \omega_{A0}$, where q_1' is the derivative of the safety factor q at the $q = 1$ surface and ω_{A0} is the toroidal Alfvén frequency at the magnetic axis. For sample parameters, $\omega_{A0} = 6.4 \times 10^6 \text{s}^{-1}$, $T_e = 6\text{keV}$, $n = 3.5 \times 10^{19}\text{m}^{-3}$ and $q_1' = 2.0\text{m}^{-1}$, corresponding to TFTR experiments that have sawtooth crashes [4, 5], we obtain $\tau_0 = 90\mu\text{s}$ and $\tau_e = 270\mu\text{s}$, although the ratio $\tau_0/\tau_e = 0.33$ can drastically change in proportion to $T_e^{-3/2}n^2$.

By recalling that the resistive layer width δ_η for the case of $\Delta' = \infty$ is given by $\delta_\eta \sim (\eta/q_1'\omega_{A0})^{1/3}$, namely, $\delta_\eta/d_e \sim (\tau_0/\tau_e)^{1/3}$, we expect the reconnection to be relatively collisionless when τ_0 is shorter than τ_e. Indeed, the nonlinear acceleration phase is observed numerically for $\tau_0/\tau_e < 1$. Figure 9 shows instantaneous growth rates of $\epsilon(t)$ for different values of resistivity $\tau_0/\tau_e(\propto \eta)$. The linear growth rate γ, which emerges at the small amplitude $\epsilon/d_e = 0.1(\ll 1)$, obeys the dispersion relation $\gamma\tau_0 = (\tau_0/\tau_e + \gamma\tau_0)^{1/3}$ obtained by asymptotic matching [28]. As the amplitude ϵ enters into the nonlinear phase $\epsilon/d_e > 1$, acceleration occurs for $\tau_0/\tau_e < 1$. Since the electron skin depth d_e is wider than the resistive layer width δ_η for $\tau_0/\tau_e < 1$, collisionless reconnection governs macroscopic fluid motion. On the contrary, for $\tau_0/\tau_e > 1$, the resistive layer initiates the reconnection process and hence deceleration occurs in figure 9, which is more like the quasi-equilibrium evolution caused by the resistive kink mode [2].

6. Summary

In this work, we have analytically elucidated the acceleration mechanism for collisionless reconnection driven by electron inertia. A variational method based on the Lagrangian description of collisionless plasma is shown to be useful especially for predicting nonlinear evolution; conventional asymptotic matching does not apply to this problem unless an exact nonlinear and unsteady solution is available around the boundary layers.

We have demonstrated the existence of a nonlinear displacement map that decreases the potential energy of the Lagrangian system into the nonlinear regime. No matter how small the electron skin depth d_e, electron inertia enables ideal fluid motion to release free energy ($\simeq$ magnetic energy) of the equilibrium state because the frozen-in flux is switched from ψ to $\psi_e = \psi - d_e^2\nabla^2\psi$, producing a reconnecting layer of width d_e. In
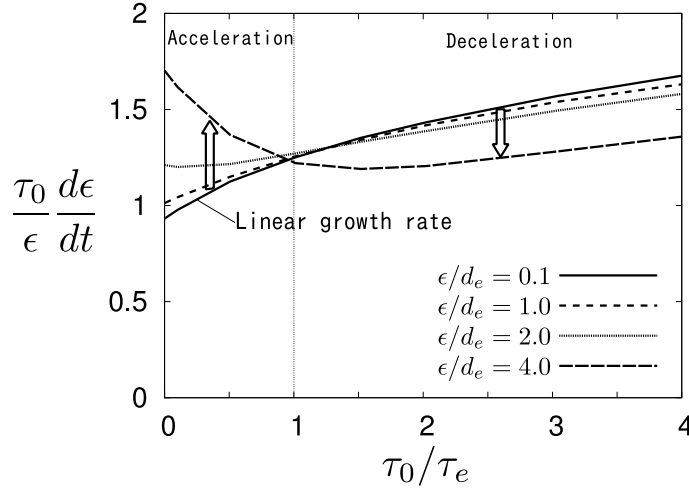
Figure 9. Instantaneous growth rates $(\tau_0/\epsilon)d\epsilon/dt$ versus resistivity τ_0/τ_e, numerically evaluated at several levels of amplitude ϵ/d_e ($d_e/L_x = 0.01$ and $L_y/L_x = 4\pi$).

the large-Δ' limit, the formation of Y-shaped structures connected by a current layer in the magnetic configuration is favorable for the steepest descent of the potential energy. This descent scales as $O(\hat{\epsilon}^3)$ for $\hat{\epsilon} = \epsilon/d_e \gg 1$ with respect to the displacement ϵ (or the island width). The associated explosive growth of ϵ would continue until ϵ reaches the system size and leads to an equilibrium collapse during a finite time $\sim \tau_0$.

Although our analytical model is too simple to explain all sawtooth physics in tokamaks, the time scale of explosion ($\tau_0 \sim 90\mu s$) that is predicted in this work is comparable to experimentally observed sawtooth collapse times [4, 5]. However, resistivity is not negligible in tokamaks and tends to decelerate the reconnection. Our simulations exhibit nonlinear acceleration only for the case of $\tau_0/\tau_e = \eta/d_e^3 q_1' \omega_{A0} < 1$, which can be fulfilled by the experiments. In more realistic plasmas, the strong current spike generated by electron inertia would cause rapid heating of the plasma, which would reduce the local resistivity η, and, what is more, would produce runaway electrons. Since these effects also act as positive feedback, we expect that sawtooth collapse occurs once the acceleration condition $\tau_0/\tau_e < 1$ is satisfied at the $q = 1$ surface.

We infer that the state of lowest potential energy is similar to Kadomtsev's fully reconnected state (where q at the magnetic axis is $q_0 = 1$) [1]. But, if dissipation were sufficiently small, it would also corresponds to the state of maximum kinetic energy, where a strong convective flow remains. As shown in numerical simulations [20, 21], such a residual flow causes a secondary reconnection and restores a magnetic field similar to the original equilibrium ($q_0 < 1$). If our analytical result is adapted to cylindrical geometry, this partial reconnection model will be corroborated theoretically.

We expect further application of our variational approach to be fruitful for describing strongly nonlinear and nonequilibrium dynamics of sawtooth collapses. As is well known, finite-Larmor-radius effects and diamagnetic effects would modify the island structure and dynamics significantly on the ion scale which is larger than d_e. Our

approach is feasible even for multiscale problems that require nested boundary layers, as long as dissipation is not the dominant factor. Extensions of the present analysis to more general two-fluid equations are in progress and will be reported elsewhere.

Acknowledgments

Appendix A. Linear stability analysis

In the ideal MHD limit $(d_e = 0)$, it is well known that the equilibrium (3) has a marginally stable eigenmode $(\gamma = 0)$ which is expressed by $\hat{\psi} = \psi_0 \cos \kappa(\alpha|x| - \pi/2)$ (where $\kappa = \sqrt{1 - k^2/\alpha^2}$) in terms of $\hat{\psi} = -\psi'\hat{\xi}$. When $k^2 < \alpha^2$, this eigenmode formally makes $W^{(2)}$ negative;

$$W^{(2)} = -2\,\hat{\psi}\hat{\psi}'\Big|_{x=-0}^{x=+0} = -2\psi_0^2\alpha\kappa\sin(\kappa\pi) < 0, \tag{A.1}$$

which also implies that the tearing index is positive, $\Delta' = \hat{\psi}'/\hat{\psi}|_{x=-0}^{x=+0} = 2\alpha\kappa\tan\kappa\frac{\pi}{2} > 0$. The corresponding $\hat{\xi} = -\hat{\psi}/\psi'$ is, however, discontinuous at $x = 0, \pm L_x/2$ and hence $I^{(2)} = \infty$. It is therefore reasonable to infer that this marginal mode would be destabilized by adding electron inertia $d_e \ll L_x$.

Note that the integrand of the potential energy (13) is composed of two quadratic terms, which are, respectively, positive and negative definite. Since $\psi'_e \simeq \psi'$ for small d_e, the main role of the electron inertia is to weaken the *magnetic tension* (equal to the former positive term) through the smoothing operator $(1 - d_e^2\nabla^2)^{-1}$.

By assuming the ordering (4) (in which $\Delta' \simeq 8\alpha^3/\pi k^2$ is *large*) and employing the test function $\hat{\xi}$ in figure 3, let us estimate only the leading-order term in (12) and (13). For that purpose, we can always use an approximation $\nabla^2 \simeq \partial_x^2$. Then, (12) easily yields the estimate of $I^{(2)}$ in (15).

To calculate the potential energy (13), we introduce a neighborhood $[-d_0, d_0]$ of the boundary layer $[-d_e, d_e]$, where d_0 is supposed to be a few times larger than d_e. The potential energy in the *outer* region $[-L_x/2 + d_0, -d_0] \cup [d_0, L_x/2 - d_0]$ is estimated by

$$W^{(2)}_{[-L_x/2+d_0,-d_0]\cup[d_0,L_x/2-d_0]} = -2\,\hat{\psi}\hat{\psi}'\Big|_{x=-d_0}^{x=d_0} \simeq -4\frac{d_0}{\tau_H^2}, \tag{A.2}$$

where $\tau_H^{-1} = \psi_0\alpha^2$, because $\hat{\psi} \simeq \psi_0\cos(\alpha|x| - \pi/2)$ in this region.

Next, we focus on the inner region $[-d_0, d_0]$ by using a local coordinate $\hat{x} = x/d_e$ and approximating the equilibrium profile by $\psi'_e \simeq \psi' \simeq -(d_e/\tau_H)\hat{x}$. For given

$$\hat{\psi}_e = -\psi'_e\hat{\xi} = \frac{d_e}{\tau_H}\begin{cases} -\hat{x}^2 & \text{for } |\hat{x}| < 1 \\ -|\hat{x}| & \text{for } 1 < |\hat{x}|, \end{cases} \tag{A.3}$$
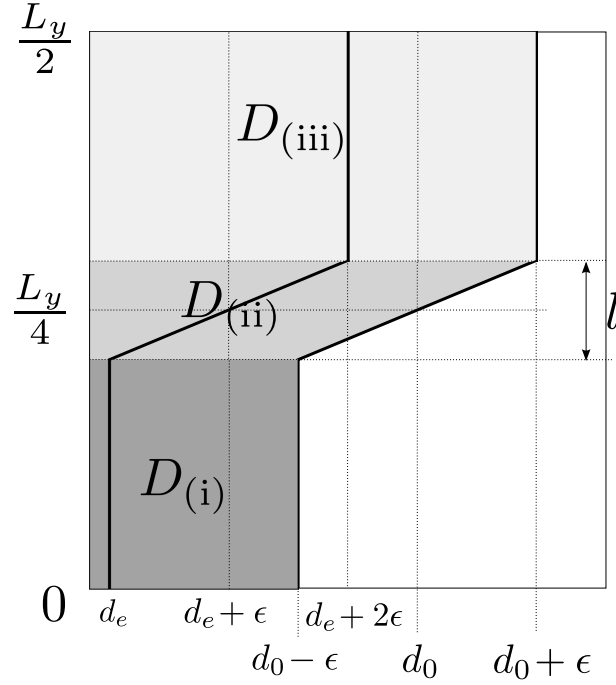
Figure B1. Closeup of three regions (i)-(iii) in figure 5

the corresponding $\hat{\psi}$ is obtained by solving $\hat{\psi}_e = \hat{\psi} - \partial_{\hat{x}}^2 \hat{\psi}$ under the boundary condition, $\hat{\psi} \to \hat{\psi}_e$ as $|\hat{x}| \to \infty$. This analysis results in

$$\hat{\psi} = \frac{d_e}{\tau_H} \begin{cases} -(\hat{x}^2 + 2) + \dfrac{3}{2}e^{-1}(e^{\hat{x}} + e^{-\hat{x}}) & |\hat{x}| < 1 \\[2mm] -|\hat{x}| + \dfrac{3e^{-1} - e}{2}e^{-|\hat{x}|} & 1 < |\hat{x}|, \end{cases} \tag{A.4}$$

where $\hat{\psi}(0) \neq 0$ indicates that this perturbation causes magnetic reconnection. The potential energy inside the layer $[-d_0, d_0]$ is calculated as

$$\begin{aligned} W^{(2)}_{[-d_0,d_0]} &\simeq \frac{1}{d_e} \int_{-d_0/d_e}^{d_0/d_e} d\hat{x} \left[|\partial_{\hat{x}} \hat{\psi}|^2 + |\partial_{\hat{x}}^2 \hat{\psi}|^2 \right] \\ &\simeq \frac{d_e}{\tau_H^2} \left(-\frac{1}{3} - 9e^{-2} + 2\frac{d_0}{d_e} \right), \end{aligned} \tag{A.5}$$

where we have neglected e^{-d_0/d_e} by making d_0 larger than d_e to some extent. Since other boundary layers at $x = \pm L_x/2$ can be treated equivalently, the total potential energy on the whole domain $[-L_x/2, L_x/2]$ is estimated as (15).

Appendix B. Estimate of potential energy change

Here we estimate change of the potential energy $W[\boldsymbol{G}_\epsilon]$ that is caused by the nonlinear displacement map $\boldsymbol{G}_\epsilon$ given in (18). In a way similar to that of the linear analysis (see Appendix A), we introduce a domain $[0, d_0] \times [0, L_y/2]$ where d_0 is now taken to be

somewhat larger than $2d_e + 2\epsilon$. This domain is deformed by the map $\boldsymbol{G}_\epsilon$ as shown in figure B1, where we refer to shrinking and expanding domains as

$$D_{(i)} = [0, d_0 - \epsilon] \times \left[0, \frac{L_y}{4} - \frac{l}{2}\right], \tag{B.1}$$

$$D_{(iii)} = [0, d_0 + \epsilon] \times \left[\frac{L_y}{4} + \frac{l}{2}, \frac{L_y}{2}\right], \tag{B.2}$$

respectively, and their intermediate domain as $D_{(ii)}$. The potential energy will not change significantly outside of these domains, because the fluid is simply subject to parallel translation along the x direction. Moreover, we are only interested in the domains $D_{(i)}$ and $D_{(iii)}$, on which efficient decrease of the potential energy is observed as follows.

Appendix B.1. Potential energy on $D_{(i)}$

The equilibrium (3) is approximated by $\psi_e^{(0)}(x) \simeq \psi^{(0)}(x) \simeq \psi_0(1 - \alpha^2 x^2/2)$ and it is deformed into $\psi_e(x, y, \epsilon) = \psi_e^{(0)}(g_\epsilon^{-1}(x))$ on $D_{(i)}$. Therefore, $\delta\psi_e = \psi_e - \psi_e^{(0)}$ is given by

$$\delta\psi_e = \frac{1}{\tau_H} \begin{cases} \dfrac{1}{2}(1 - e^{2\hat{\epsilon}})x^2 & \text{for } 0 < x < d_e e^{-\hat{\epsilon}} \\[2mm] -\dfrac{1}{2}\left[d_e\left(\log\dfrac{x}{d_e} + 1\right) + \epsilon\right]^2 + \dfrac{x^2}{2} & \text{for } d_e e^{-\hat{\epsilon}} < x < d_e \\[2mm] -\epsilon x - \dfrac{\epsilon^2}{2} & \text{for } d_e < x. \end{cases} \tag{B.3}$$

For large $\hat{\epsilon} = \epsilon/d_e \gg 1$, we can neglect the innermost region $0 < x < d_e e^{-\hat{\epsilon}}$ and the asymptotic form of $\delta\psi_e$ contains a logarithmic function as follows.

$$\delta\psi_e = \frac{d_e^2}{\tau_H} \begin{cases} -(1 + \hat{\epsilon})\log\hat{x} - \dfrac{1}{2}(1 + \hat{\epsilon})^2 + \dfrac{\hat{x}^2}{2} & \text{for } 0 < \hat{x} < 1 \\[2mm] -\hat{\epsilon}\hat{x} - \dfrac{\hat{\epsilon}^2}{2} & \text{for } 1 < \hat{x}, \end{cases} \tag{B.4}$$

where $\hat{x} = x/d_e$, and the corresponding spike is recognized in figure 6(i). By solving $(1 - \partial_{\hat{x}}^2)\delta\psi = \delta\psi_e$ for $\delta\psi$, the change of current $\delta J = -\partial_x^2(\delta\psi)$ turns out to be

$$\delta J = \frac{1}{\tau_H} \begin{cases} -(\hat{\epsilon} + 1)\mathrm{E_c}(\hat{x}) - 1 + c_1\cosh(\hat{x}) & \text{for } 0 < \hat{x} < 1 \\[2mm] c_2 e^{-\hat{x}} & \text{for } 1 < \hat{x}, \end{cases} \tag{B.5}$$

where we have defined $\mathrm{E_c}(x) = [e^x\mathrm{E_i}(-x) + e^{-x}\mathrm{E_i}(x)]/2$ using the exponential integral $\mathrm{Ei}(x) = \mathrm{p.v.}\int_{-\infty}^{x}(e^s/s)ds$. The coefficients c_1 and c_2 are matching data at the interface $\hat{x} = 1$, which are linear functions of $\hat{\epsilon}$ as follows;

$$c_1(\hat{\epsilon}) = \frac{(\hat{\epsilon} + 1)[\mathrm{E_c}'(1) + \mathrm{E_c}(1)] + 1}{e}, \tag{B.6}$$

$$c_2(\hat{\epsilon}) = (\hat{\epsilon} + 1)\left[\cosh(1)\mathrm{E_c}'(1) - \sinh(1)\mathrm{E_c}(1)\right] - \sinh(1). \tag{B.7}$$

Since $\mathrm{E_c}(\hat{x}) \simeq \log|\hat{x}|$ near $\hat{x} = 0$, a strong current spike develops in the form of logarithmic function, as noted earlier in Ref. [9]. However, the asymptotic form of

$\delta J = J - J^{(0)}$ remains square-integrable and, hence, the current energy change in (9) is, at most, of the second order;

$$\frac{1}{2}\int_0^{d_0} d_e^2(|J|^2 - |J^{(0)}|^2)dx = \frac{d_e^3}{\tau_H^2} \times O(\hat{\epsilon}^2).$$ (B.8)

On the other hand, the magnetic flux $\psi = \psi^{(0)} + \delta\psi$ is free from such logarithmic singularity and its derivative,

$$\partial_x\psi = \frac{d_e}{\tau_H}\begin{cases} -(1+\hat{\epsilon})\partial_{\hat{x}}\left[\log\hat{x} - \mathrm{E}_c(\hat{x})\right] - c_1\sinh(\hat{x}) & \text{for } 0 < \hat{x} < 1 \\ -(\hat{x}+\hat{\epsilon}) + c_2 e^{-\hat{x}} & \text{for } 1 < \hat{x}, \end{cases}$$ (B.9)

is again square-integrable and linearly depends on $\hat{\epsilon}$. Hence, the leading-order estimate of magnetic energy is simply

$$\frac{1}{2}\int_0^{d_0-\epsilon}|\partial_x\psi|^2 dx = \frac{d_e^3}{\tau_H^2}\left[\frac{1}{2}\int_1^{(d_0/d_e)-\hat{\epsilon}}(\hat{x}+\hat{\epsilon})^2 d\hat{x} + O(\hat{\epsilon}^2)\right]$$

$$= \frac{1}{\tau_H^2}\left[\frac{d_0^3}{6} - \frac{\epsilon^3}{6} + O(\hat{\epsilon}^2 d_e^3)\right],$$ (B.10)

which decreases as $\hat{\epsilon}^3$ for $\hat{\epsilon} \gg 1$. This decrease of the magnetic energy dominates the increase of current energy (B.8). Therefore, the potential energy change on $D_{(i)}$ is found to be

$$\delta W_{(i)} = \left(\frac{L_y}{4} - \frac{l}{2}\right)\frac{1}{\tau_H^2}\left[-\frac{\epsilon^3}{6} + O(\hat{\epsilon}^2 d_e^3)\right].$$ (B.11)

Appendix B.2. Potential energy on $D_{(iii)}$

For the purpose of estimating δW on $D_{(iii)}$ to leading order, one may approximate the inverse map of (18) as

$$x_0 = \begin{cases} \dfrac{x}{2} & \text{for } 0 < x < 2\epsilon \\ x - \epsilon & \text{for } 2\epsilon < x, \end{cases}$$ (B.12)

for large $\hat{\epsilon}$. The equilibrium flux $\psi_e^{(0)}(x) \simeq \psi_0(1 - \alpha^2 x^2/2)$ is expanded by this outflow and is deformed into a flat-topped shape [see figure 6(iii)]. In the same manner as for the domain $D_{(i)}$, we first obtain

$$\delta\psi_e = \frac{1}{\tau_H}\begin{cases} \dfrac{3x^2}{8} & \text{for } 0 < x < 2\epsilon \\ \dfrac{2\epsilon x - \epsilon^2}{2} & \text{for } 2\epsilon < x, \end{cases}$$ (B.13)

and calculate the current change as follows:

$$\delta J = \frac{1}{\tau_H}\begin{cases} -\dfrac{3}{4} + \left(\dfrac{\hat{\epsilon}}{2} + \dfrac{3}{4}\right)\dfrac{1}{2}e^{\hat{x}-2\hat{\epsilon}} & \text{for } 0 < x < 2\epsilon \\ \left(\dfrac{\hat{\epsilon}}{2} - \dfrac{3}{4}\right)\dfrac{1}{2}e^{-\hat{x}+2\hat{\epsilon}} & \text{for } 2\epsilon < x. \end{cases}$$ (B.14)

By keeping the smallness of $e^{-\hat{\epsilon}}$ in mind, we confirm that the current energy change is again of the second order $O(\hat{\epsilon}^2)$. The asymptotic form of $\partial_x \psi$ is estimated by

$$\partial_x \psi = \frac{d_e}{\tau_H} \begin{cases} -\dfrac{\hat{x}}{4} - \left(\dfrac{\hat{\epsilon}}{2} + \dfrac{3}{4}\right) \dfrac{1}{2} e^{\hat{x}-2\hat{\epsilon}} & \text{for } 0 < x < 2\epsilon \\[3mm] -(\hat{x} - \hat{\epsilon}) + \left(\dfrac{\hat{\epsilon}}{2} - \dfrac{3}{4}\right) \dfrac{1}{2} e^{-\hat{x}+2\hat{\epsilon}} & \text{for } 2\epsilon < x, \end{cases} \tag{B.15}$$

and the magnetic energy is also found to decrease as $\hat{\epsilon}^3$;

$$\frac{1}{2} \int_0^{d_0+\epsilon} |\partial_x \psi|^2 dx = \frac{d_e^3}{2\tau_H^2} \left[\int_0^{2\hat{\epsilon}} \frac{\hat{x}^2}{16} d\hat{x} + \int_{2\hat{\epsilon}}^{d_0/d_e+\hat{\epsilon}} (\hat{x} - \hat{\epsilon})^2 d\hat{x} + O(\hat{\epsilon}^2) \right]$$

$$= \frac{1}{\tau_H^2} \left[\frac{d_0^3}{6} - \frac{\epsilon^3}{12} + O(\hat{\epsilon}^2 d_e^3) \right]. \tag{B.16}$$

The flat-topped region of $\psi_e(\simeq \psi)$ corresponds to the magnetic island, on which the magnitude of $\partial_x \psi$ obviously decreases. The potential energy on $D_{\text{(iii)}}$ therefore decreases as follows:

$$\delta W_{\text{(iii)}} = \left(\frac{L_y}{4} - \frac{l}{2}\right) \frac{1}{\tau_H^2} \left[-\frac{\epsilon^3}{12} + O(\hat{\epsilon}^2 d_e^3) \right]. \tag{B.17}$$

Appendix C. Estimate of kinetic energy

Here we estimate the kinetic energy $K[\boldsymbol{G}_{\epsilon(t)}]$ of the displacement map $\boldsymbol{G}_{\epsilon(t)}$ given in (18), where only $\epsilon(t)$ is assumed to be time-dependent. By invoking figure B1 again, the dominant part of kinetic energy turns out to exist in the domains $D_{\text{(i)}}$, $D_{\text{(ii)}}$ and $D_{\text{(iii)}}$. Since $D_{\text{(ii)}}$ is ignored in this work (by assuming $l \ll L_y$), we exhibit only the results for $D_{\text{(i)}}$ and $D_{\text{(iii)}}$ as follows.

Appendix C.1. Kinetic energy on $D_{\text{(i)}}$

Owing to our special choice of g_ϵ, the x-component of the velocity field on $D_{\text{(i)}}$ is simply given by

$$v_x(x, y, \epsilon) = \frac{d\epsilon}{dt} \frac{dg_\epsilon}{d\epsilon}(g_\epsilon^{-1}(x)) = \frac{d\epsilon}{dt} \begin{cases} -\dfrac{x}{d_e} & \text{for } 0 < x < d_e \\[3mm] -1 & \text{for } d_e < x. \end{cases} \tag{C.1}$$

By solving the incompressibility condition $\partial_x v_x + \partial_y v_y = 0$ under appropriate boundary conditions, the y-component of the velocity field is found to be

$$v_y(x, y, \epsilon) = \frac{d\epsilon}{dt} \begin{cases} \dfrac{y}{d_e} & \text{for } 0 < x < d_e \\[3mm] 0 & \text{for } d_e < x. \end{cases} \tag{C.2}$$

This v_y dominantly contributes to the kinetic energy on $D_{\text{(i)}}$, which is readily estimated by

$$K_{\text{(i)}} = \int_0^{\frac{L_y}{4}-\frac{l}{2}} dy \int_0^{d_0-\epsilon} dx \frac{1}{2}(v_x^2 + v_y^2) \simeq \frac{1}{6d_e} \left(\frac{L_y}{4} - \frac{l}{2}\right)^3 \left(\frac{d\epsilon}{dt}\right)^2. \tag{C.3}$$

Appendix C.2. Kinetic energy on $D_{\text{(iii)}}$

We can go through the same procedures as for $D_{\text{(i)}}$, but the analysis is somewhat complicated by the fact that the inverse map $x \mapsto x_0$ should be dealt with as an implicit function. In terms of the *unperturbed* position x_0, the velocity field is expressed by

$$v_x(x, y, \epsilon) = \frac{d\epsilon}{dt} \frac{\partial x}{\partial \epsilon}(x_0) = \frac{d\epsilon}{dt} \begin{cases} \hat{x}_0 e^{-\hat{\epsilon}} & \text{for } 0 < x_0 < d_e \\ e^{\hat{x}_0 - \hat{\epsilon} - 1} & \text{for } d_e < x_0 < d_e + \epsilon \\ 1 & \text{for } d_e + \epsilon < x_0, \end{cases} \qquad (C.4)$$

$$v_y(x, y, \epsilon) = \left(\frac{L_y}{2} - y\right) \frac{d\epsilon}{dt} \frac{1}{d_e} \begin{cases} \dfrac{e^{-\hat{\epsilon}}}{2 - e^{-\hat{\epsilon}}} & \text{for } 0 < x_0 < d_e \\ \dfrac{e^{\hat{x}_0 - \hat{\epsilon} - 1}}{2 - e^{\hat{x}_0 - \hat{\epsilon} - 1}} & \text{for } d_e < x_0 < d_e + \epsilon \\ 0 & \text{for } d_e + \epsilon < x_0. \end{cases} \qquad (C.5)$$

Using the change of variables from x to x_0, the kinetic energy on $D_{\text{(iii)}}$ is therefore estimated as

$$\begin{aligned} K_{\text{(iii)}} &= \int_{\frac{L_y}{4} + \frac{l}{2}}^{\frac{L_y}{2}} dy \int_0^{d_0} dx_0 \frac{1}{2}(v_x^2 + v_y^2) \frac{\partial x}{\partial x_0} \\ &\simeq \frac{2\log 2 - 1}{6d_e} \left(\frac{L_y}{4} - \frac{l}{2}\right)^3 \left(\frac{d\epsilon}{dt}\right)^2, \end{aligned} \qquad (C.6)$$

where we have neglected $e^{-\hat{\epsilon}}$ for large $\hat{\epsilon} \gg 1$.

References

[1] Kadomtsev B.B. 1975 *Sov. J. Plasma Phys.* **1** 389
[2] Waelbroeck F.L. 1989 *Phys. Fluids B* **1** 2372
[3] Soltwisch H. 1988 *Rev. Sci. Instrum* **59** 1599
[4] Levinton F.M., Batha S.H., Yamada M. and Zarnstorff M.C. 1993 *Phys. Fluids B* **5** 2554
[5] Yamada M., Levinton F.M., Pomphrey N., Budny R., Manickam J. and Nagayama Y. 1994 *Phys. Plasmas* **1** 3269
[6] Basu B. and Coppi B. 1981 *Phys. Fluids* **24** 465
[7] Porcelli F. 1991 *Phys. Rev. Lett.* **66** 425
[8] Aydemir A.Y. 1992 *Phys. Fluids B* **4** 2469
[9] Ottaviani M. and Porcelli F. 1993 *Phys. Rev. Lett.* **71** 3802
[10] Matsumoto T., Naitou H., Tokuda S. and Kishimoto Y. 2005 *Phys. Plasmas* **12** 092505
[11] Rosenbluth M.N., Dagazian R.Y. and Rutherford P.H. 1973 *Phys. Fluids* **16** 1894
[12] Rutherford P.H. 1973 *Phys. Fluids* **16** 1903
[13] Cafaro E., Grasso D., Pegoraro F., Porcelli F. and Saluzzi A. 1998 *Phys. Rev. Lett.* **80** 4430
[14] Grasso D., Califano F., Pegoraro F. and Porcelli F. 1999 *Plasma Phys. Control. Fusion* **41** 1497
[15] Tassi E., Morrison P.J., Grasso D. and Pegoraro F. 2010 *Nucl. Fusion* **50** 034007
[16] Bernstein I.B., Frieman E.A., Kruskal M.D. and Kulsrud R.M. 1958 *Proc. R. Soc. Lond. A* **244** 17
[17] Hain K., Lüst R. and Schlüter A. 1957 *Z. Naturforsch.* **12a**, 833
[18] Morrison, P.J. 2009 *American Institute of Physics Conf. Proc.* **1188**, 329
[19] Wesson J.A. 1990 *Nucl. Fusion* **30** 2545
[20] Biskamp D. and Drake J.F. 1994 *Phys. Rev. Lett.* **73** 971

[21] Naitou H., Tsuda K., Lee W.W. and Sydora R.D. 1995 *Phys. Plasmas* **2** 4257
[22] Newcomb W.A. 1962 *Nucl. Fusion Suppl.* Pt.2 451
[23] Morrison P.J. 1998 *Rev. Mod. Phys.* **70** 467
[24] Padhye N. and Morrison P.J. 1996 *Plasma Phys. Repts.* **22** 869
[25] Syrovatskii S.I. 1971 *Sov. Phys. JETP* **33** 933
[26] Hirota M. 2011 *J. Plasma Phys.* **77** 589
[27] Haney S.W. and Freidberg J.P. 1989 *Phys. Fluids B* **1** 1637
[28] Biskamp D. 2000 *Magnetic Reconnection in Plasmas* (Cambridge: Cambridge University Press) p 227